Study of the performance of $CsPbBr_3$ perovskite solar cells by chlorobenzene additive

A. DONG, J. DONG*
School of Science, China University of Geosciences, Beijing, 100083, China

All-inorganic $CsPbBr_3$ perovskite solar cells have garnered widespread attention due to their excellent stability. However, the $CsPbBr_3$ perovskite light-absorbing layer suffers from several critical issues, including a large bandgap (~2.3 eV), a narrow light absorption range, and severe charge recombination, which significantly hinder the improvement of its power conversion efficiency (PCE). In this study, additive engineering was employed using a commonly used anti-solvent, chlorobenzene (CB), as an additive to fabricate $CsPbBr_3$ perovskite solar cells. By regulating the growth process of the perovskite films, the crystallinity of $CsPbBr_3$ perovskite films was effectively optimized, resulting in highly efficient and stable perovskite films. The device treated with chlorobenzene achieved a PCE of 9.28% and maintained over 90% of its initial efficiency after 120 days of storage in air under unencapsulated conditions.

(Received March 20, 2025; accepted October 10, 2025)

Keywords: $CsPbBr_3$, Chlorobenzene, Additive, Perovskite solar cells

1. Introduction

Compared to organic-inorganic hybrid perovskite materials, all-inorganic $CsPbBr_3$ (X = Cl, Br, or I) perovskite materials exhibit more stable structures. Among all-inorganic $CsPbX_3$ perovskite solar cell systems, $CsPbBr_3$ perovskite solar cells show superior temperature and humidity stability and can be fabricated in air. Unencapsulated $CsPbBr_3$ perovskite solar cells can maintain high efficiency even after 30 days of storage in air [1]. However, $CsPbBr_3$ perovskite materials suffer from a large bandgap (~2.3 eV), a narrow light absorption range, and severe charge recombination, which significantly limit the improvement of their power conversion efficiency (PCE) [2-4].

Hodes et al. were the first to use $CsPbBr_3$ as the light-absorbing layer for solar cells, achieving a PCE of 5.95% and an open-circuit voltage of 1.28 V [5]. Subsequently, Liu et al. fabricated all-inorganic $CsPbBr_3$ perovskite solar cells with carbon electrodes, demonstrating good tolerance to humid environments and extreme temperatures, achieving a PCE of 6.7% [6]. Tang's group further improved the PCE of the devices to 10.6% through interface engineering and compositional regulation [7,8]. Despite these achievements, the $CsPbBr_3$ perovskite absorbing layer still suffers from severe non-radiative recombination and a high density of grain boundary defects, which hinder further improvement in device performance [9, 10].

The morphology and crystalline quality of the perovskite absorbing layer directly influence the performance of perovskite solar cells [11-14]. To improve the crystallinity and film morphology of perovskite thin films, commonly used methods include interface engineering, anti-solvent engineering, and additive engineering. Among these, interface engineering only passivates the surface of the perovskite thin film and cannot address defects within the perovskite bulk [15]. Anti-solvent engineering involves a complex fabrication process and requires high precision in experiment parameters, such as volume of anti-solvent, dripping time, and temperature [16-20]. In contrast, additive engineering involves simply introducing appropriate additives into the perovskite precursor solution, thereby improving the film quality by regulating the crystal growth process of the perovskite. This method is relatively simple to implement experimentally [21-24]. Chlorobenzene (CB), as a common solvent, has high density and high boiling point. Using CB as an additive is expected to be regulated the nucleation and crystallization process of perovskite films.

In this study, additive engineering was employed to fabricate $CsPbBr_3$ perovskite solar cells using CB as the additive. By regulating the growth process of the perovskite thin films, the crystalline quality of $CsPbBr_3$ perovskite thin films was optimized, resulting in high-efficiency and stable $CsPbBr_3$ perovskite thin films. The device treated with chlorobenzene achieved a power conversion efficiency (PCE) of 9.28% and retained over 90% of its initial efficiency after 120 days of storage in air under unencapsulated conditions.

2. Experimental section

The perovskite solar cells (PSCs) in this study utilized titanium dioxide (TiO_2) as the electron transport layer, carbon as both the hole transport layer and back electrode, and $CsPbBr_3$ films as the absorber layer. All procedures were conducted in an ambient air environment.

2.1. Materials and reagents

Chlorobenzene was purchased from Xi'an Baolaite Optoelectronics Technology Co., Ltd. All other materials and reagents are detailed in a previously published work by our research group [25].

2.2. Device fabrication

Fluorine-doped tin oxide (FTO) conductive glass was chosen as the substrate, and compact titanium dioxide layer and mesoporous titanium dioxide layer, as the electron transfer layer (ETL), were synthesized on the FTO substrate via a conventional process. $CsPbBr_3$ perovskite layers are prepared by the multi-step spin-coating method on the substrates with ETL. Finally, the carbon electrode was mask scraped on the perovskite layers. The whole process was finished in ambient air, and each battery electrode area is fixed on 0.1 cm^2. The fabrication process of all PSCs in this study is described in detail in our previously published article [25].

2.3. Fabrication of CB-treated devices

Chlorobenzene (CB) was added to a prepared $PbBr_2$/N, N-Dimethylformamide (DMF) precursor solution at concentrations of 2 vol%, 4 vol%, 6 vol%, and 8 vol%. The mixed solution was then stirred at a constant temperature in a 70 °C oil bath. The remaining steps for fabricating $CsPbBr_3$ films followed the same process as described in our previously published work and are not repeated here [25]. After the $CsPbBr_3$ films were fabricated, low-temperature conductive carbon paste was blade-coated onto the films using a shadow mask, followed by annealing on a 100 °C hot plate for 20 minutes. This process yielded CB-treated $CsPbBr_3$ perovskite solar cells. The effective electrode area of each small cell was 0.1 cm^2, and all experimental procedures were carried out in an air environment.

3. Results and discussion

In this study, the annealing temperature used for preparing $PbBr_2$ films was set at 90 °C. The solvent for the $PbBr_2$ solution was DMF, which has a boiling point of 152 °C. As a result, during the annealing process, $PbBr_2$ crystallizes slowly and steadily, forming a thick and dense $PbBr_2$ film with a small amount of porosity. By adding chlorobenzene (CB), a high-boiling-point (131 °C), highly volatile solvent with low solubility for $PbBr_2$, to the $PbBr_2$/DMF precursor solution, the $PbBr_2$ solution becomes supersaturated during the spin-coating process. This accelerates the nucleation and crystallization of $PbBr_2$, resulting in a relatively loose, porous $PbBr_2$ film. Such a structure facilitates sufficient contact and reaction between the subsequent CsBr solution and the $PbBr_2$ layer, enabling the formation of higher-quality $CsPbBr_3$ films.

3.1. Effect of CB treatment on perovskite films

To investigate the morphological changes of $PbBr_2$ films before and after treatment with different concentrations of CB, SEM characterization was performed, and the results are shown in Fig. 1. Fig. 1(a) displays the SEM image of a $PbBr_2$ film without CB treatment, while Figs. 1(b–e) show SEM images of $PbBr_2$ films treated with CB concentrations of 2 vol%, 4 vol%, 6 vol%, and 8 vol%, respectively. From the images, it is evident that CB treatment introduces more porous structures into the $PbBr_2$ films. These pores facilitate sufficient contact and reaction between the subsequent CsBr solution and the $PbBr_2$ layer and provide greater space for the expansive growth of $CsPbBr_3$ crystals. Clearly, CB treatment promotes heterogeneous nucleation of $PbBr_2$, resulting in numerous $PbBr_2$ nuclei. At a CB concentration of 6 vol%, the $PbBr_2$ film exhibits the highest pore density with uniform distribution.

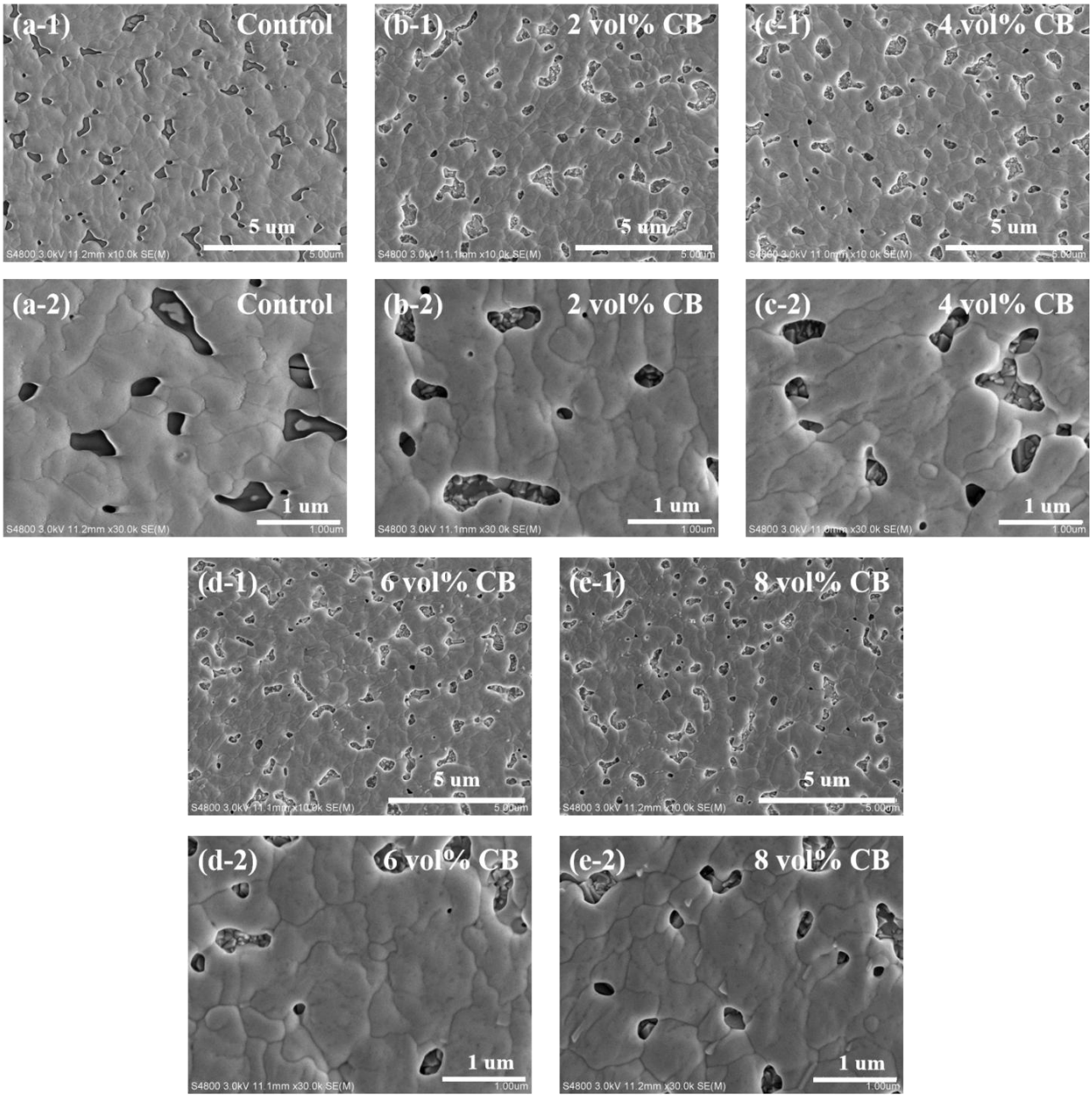

Fig. 1. SEM images of $PbBr_2$ films treated with different CB concentration

To further verify the effect of CB treatment on the crystallization of $PbBr_2$ films, XRD characterization was performed on $PbBr_2$ films before and after CB treatment, and the results are shown in Fig. 2. It can be observed that the diffraction peak positions of the $PbBr_2$ films in the control group and those treated with different CB concentrations are identical, indicating that CB participated in the crystallization process but did not incorporate into the $PbBr_2$ lattice.

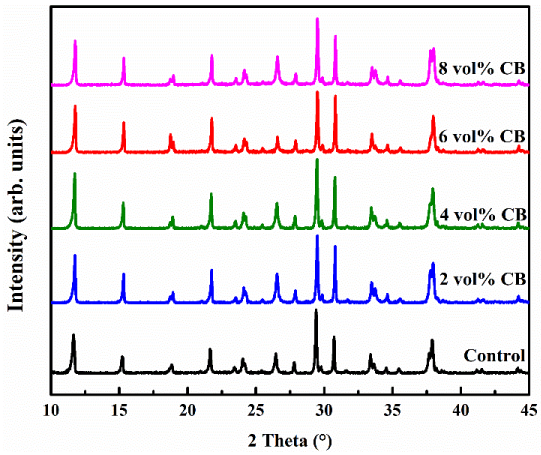

Fig. 2. XRD patterns of $PbBr_2$ films prepared with different amounts of CB (colour online)

To characterize the impact of $PbBr_2$ film morphology on $CsPbBr_3$ films, SEM analysis was conducted on $CsPbBr_3$ films, with the results shown in Fig. 3. Fig. 3(a) presents the SEM image of the control group $CsPbBr_3$ film, while Figs. 3(b–e) show SEM images of $CsPbBr_3$ films treated with CB concentrations of 2 vol%, 4 vol%, 6 vol%, and 8 vol%, respectively. As observed in Fig. 3(a), the control group $CsPbBr_3$ film exhibits low coverage with numerous pores. In contrast, the $CsPbBr_3$ films treated with CB display higher substrate coverage, significantly reduced porosity, increased grain size, and decreased grain boundaries. At a CB concentration of 6 vol%, the $CsPbBr_3$ film is the most compact and uniform, with no visible pores and the largest grain size. Therefore, using CB as an additive can effectively modify the morphology of $PbBr_2$ films, thereby improving the surface morphology of $CsPbBr_3$ films.

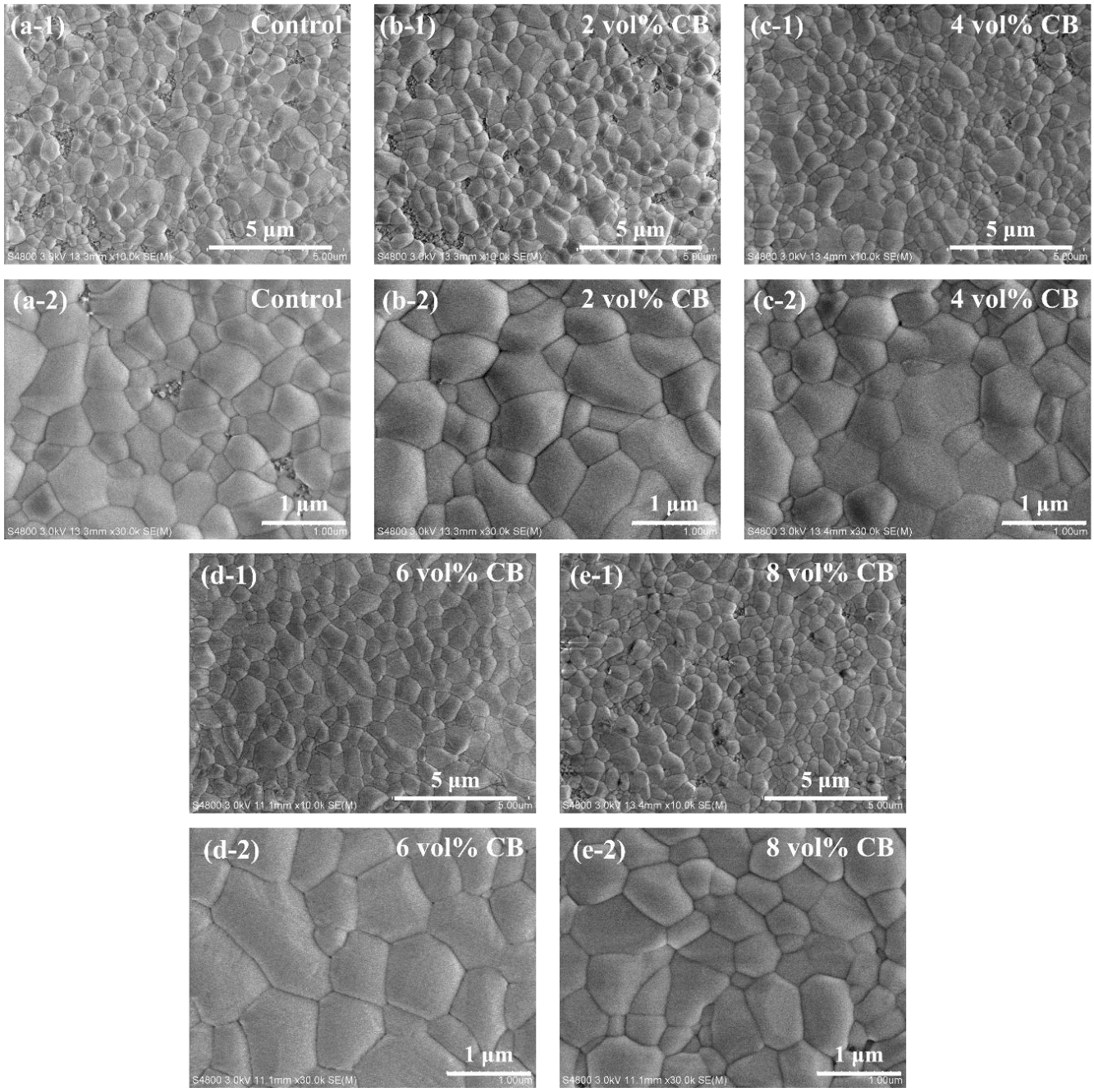

Fig. 3. SEM images of $CsPbBr_3$ films treated with different CB concentration

Fig. 4 shows the XRD patterns of perovskite films before and after CB treatment. By comparing with standard diffraction data, the peaks at 15.18°, 21.55°, 30.64°, 34.37°, and 37.76° correspond to the (100), (110), (200), (210), and (211) diffraction planes of $CsPbBr_3$ crystals, respectively. A comparison of the XRD spectra of different samples reveals that the diffraction peaks and positions of $CsPbBr_3$ crystals are identical between untreated and CB-treated samples, indicating that CB treatment does not alter the crystal structure of the perovskite layer. The primary difference lies in the suppression of the (002) diffraction peak of the $CsPb_2Br_5$ phase at 11.65° after CB treatment, while the (110) diffraction peak of the $CsPbBr_3$ phase at 21.55° is significantly enhanced. This suggests that CB treatment induces a partial phase transition from $CsPb_2Br_5$ to $CsPbBr_3$ and promotes preferential growth of the $CsPbBr_3$ crystal structure along the (110) plane. At a CB concentration of 6 vol%, the (110) diffraction peak of the $CsPbBr_3$ film is the strongest, while other secondary phase peaks are weakest, indicating that the crystallinity of the $CsPbBr_3$ film is optimal at this concentration.

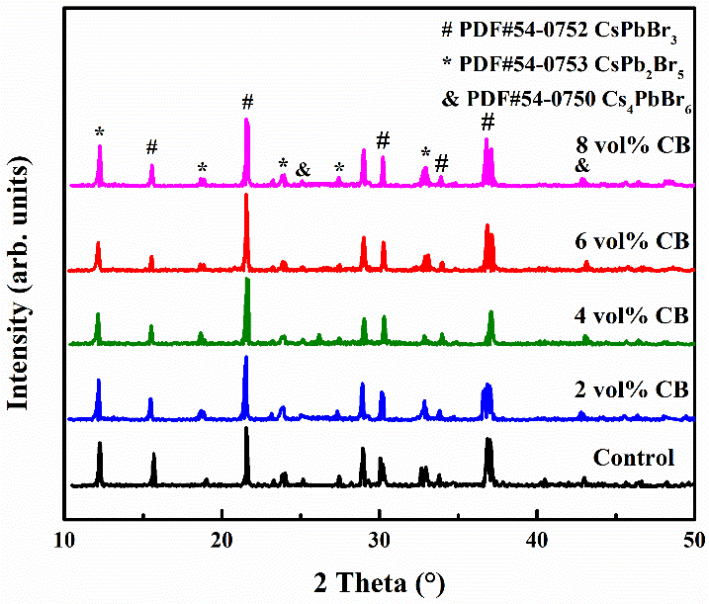

Fig. 4. XRD patterns of films prepared with different amounts of CB (colour online)

To further investigate the effect of CB treatment on the perovskite layer, XPS characterization was performed on $CsPbBr_3$ films before and after CB treatment, and the results are shown in Fig. 5. Figs. 5(a–c) display the high-resolution XPS spectra of Br 3d, Cs 3d, and Pb 4f, respectively. The data were analyzed using Origin software, revealing that after CB treatment, the Cs 3d and Pb 4f peaks exhibited a blue shift. Specifically, the $4f_{7/2}$ peak shifted from 138.2 eV to 138.4 eV, while the Cs $3d_{5/2}$ peak shifted from 724.2 eV to 724.4 eV. This indicates that the A-site ions and BX_6 octahedral structure in the perovskite film are more stably preserved, and CB treatment passivates free Pb^{2+} and Cs^+ ions in the $CsPbBr_3$ film, thereby reducing the defect density in the film [26]. Studies have shown that stronger interactions within perovskite crystals can increase formation energy, which in turn affects relative stability, crystallization kinetics, and energy level distribution [27]. Thus, the additive CB influences the growth process of $CsPbBr_3$ perovskite by regulating the growth of the $PbBr_2$ film, thereby optimizing the morphology and enhancing the stability of the perovskite, leading to a more stable $CsPbBr_3$ perovskite crystal structure.

Fig. 5(d) shows the changes in the binding energy of $CsPbBr_3$ films before and after CB treatment in the range of 120–240 eV. No Cl-related peaks (binding energy range: 195–211 eV) were observed, indicating that CB completely volatilizes after the formation of the $CsPbBr_3$ film. This demonstrates that CB solely regulates the perovskite growth process and does not remain in the $CsPbBr_3$ perovskite fil.

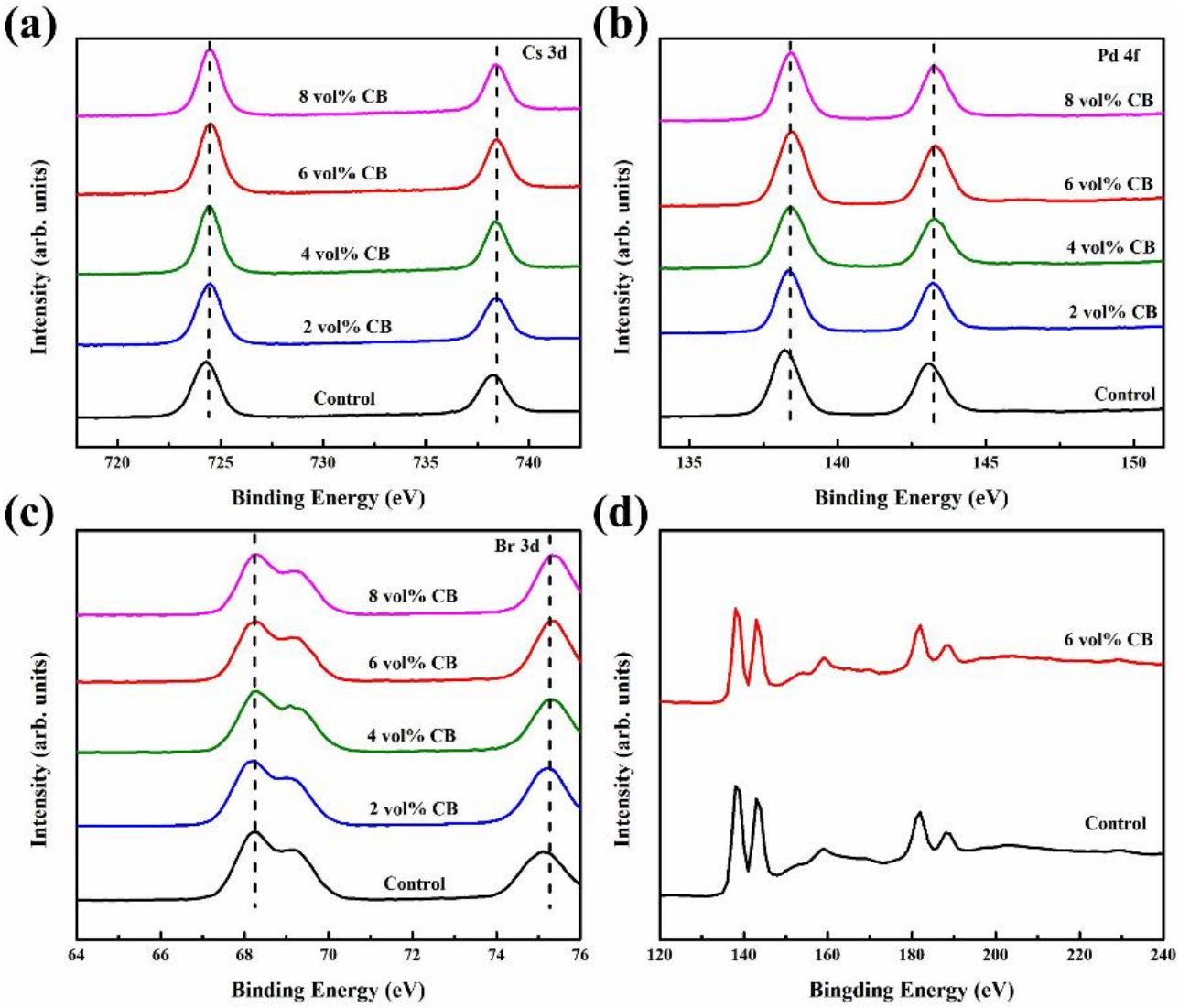

Fig. 5. XPS spectra of $CsPbBr_3$ films prepared with different amounts of CB: (a)-(c) correspond to the high-resolution XPS spectra of Cs 3d, Pb 4f and Br 3d, respectively; (d) XPS full spectrum (colour online)

To better investigate the optical properties of $CsPbBr_3$ films, UV-vis and PL measurements were conducted on $CsPbBr_3$ films before and after CB treatment, as shown in Fig. 6. From Fig. 6(a), it can be observed that the light absorption of $CsPbBr_3$ films significantly improves after CB treatment, indicating an enhanced light-harvesting capability of the device. This improvement can be attributed to the increased phase purity of $CsPbBr_3$ films post-treatment. Furthermore, a slight redshift in the absorption edge is evident, with the edge shifting from 534.3 nm to 528.3 nm, suggesting a minor reduction in the bandgap of the $CsPbBr_3$ films after CB treatment. However, the bandgap values for all films remain within the range of 2.30–2.35 eV, indicating that CB treatment has negligible influence on the bandgap of $CsPbBr_3$ films [24].

Additionally, steady-state PL measurements were performed on the $CsPbBr_3$ films, and the results are presented in Fig. 6(b). The samples used for testing consisted solely of $CsPbBr_3$ films without carrier transport layers; thus, stronger PL peaks indicate fewer defects within the films. From the PL spectra, it is evident that the CB-treated $CsPbBr_3$ films exhibit stronger PL peaks, and the PL peak position shifts from 534.3 nm to 528.3 nm, consistent with the UV-vis results. The shift in the peak position (absorption edge) can be attributed to a reduction in near-band-edge defects in the $CsPbBr_3$ films. These findings suggest that the CB additive treatment enhances the crystallinity of the $CsPbBr_3$ films, effectively reduces defects, and thereby lowers non-radiative recombination within the films.

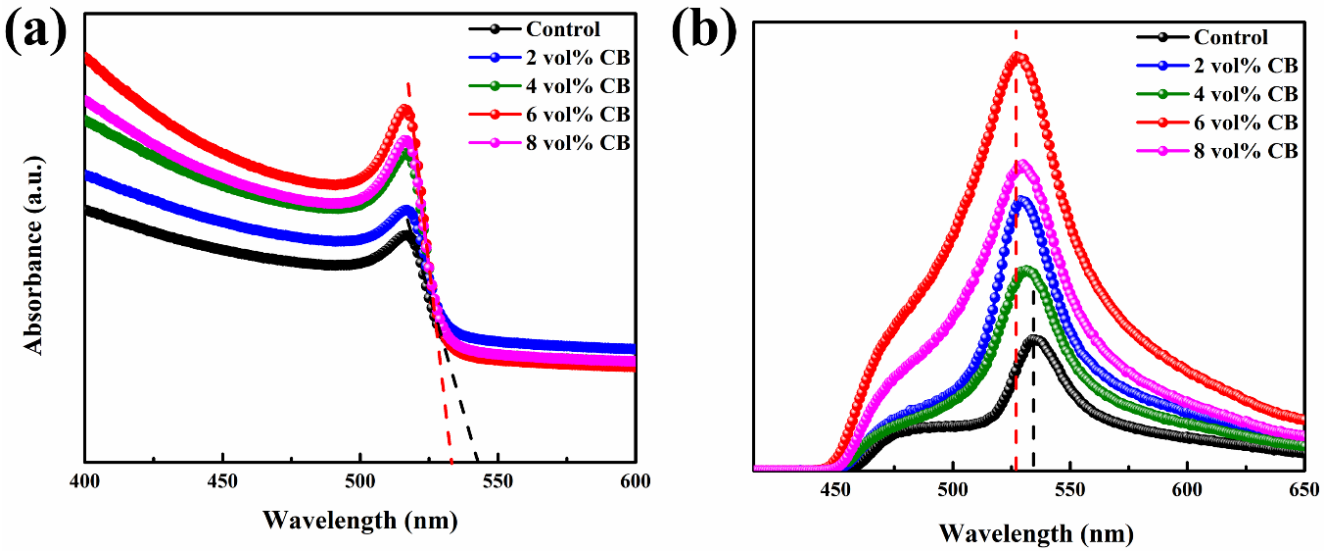

Fig. 6. (a) UV-vis spectra and (b) steady-state PL spectra of $CsPbBr_3$ films prepared with different amounts of CB (colour online)

3.2. Effect of CB treatment on perovskite solar cells

Based on the aforementioned $CsPbBr_3$ films, n-i-p mesoporous perovskite solar cells were fabricated, with the specific structure shown in Fig. 7(a). To investigate the impact of CB as an additive on device performance, current-voltage (I-V) characteristics of the devices before and after CB treatment were measured, as presented in Fig. 7(b). Detailed photovoltaic parameters are summarized in Table 1. From the figure, it can be observed that the power conversion efficiency (PCE) of the device significantly improved after CB treatment, increasing from 7.38% to 9.28%. The enhancement in efficiency mainly stems from improvements in short-circuit current density (J_{SC}) and fill factor (FF). Specifically, J_{SC} increased from 8.24 mA/cm² to 8.61 mA/cm², and FF rose from 68% to 80%. It is inferred that the use of the CB additive improved the crystallinity and coverage of the $CsPbBr_3$ films, reduced the defect state density in the perovskite absorber layer, suppressed non-radiative recombination of charge carriers, and enhanced charge carrier separation and extraction efficiency, thereby increasing J_{SC}. Moreover, the improved crystallinity and coverage, along with the reduced defects in the $CsPbBr_3$ films, contributed to a decrease in series resistance, resulting in a higher fill factor.

In addition, transient V_{OC} response measurements were conducted on the devices before and after CB treatment to characterize their photoresponse performance, with the results shown in Figs. 7(c) and (d). Clearly, the devices treated with CB exhibited a more sensitive V_{OC} response. It has been reported that slow photoresponse is often caused by a high defect state density at the surface and interfaces of perovskite films [28, 29]. The enhanced V_{OC} response after CB treatment indicates that the CB additive plays a critical role in reducing the defect state density of the $CsPbBr_3$ films, which is consistent with the results discussed earlier.

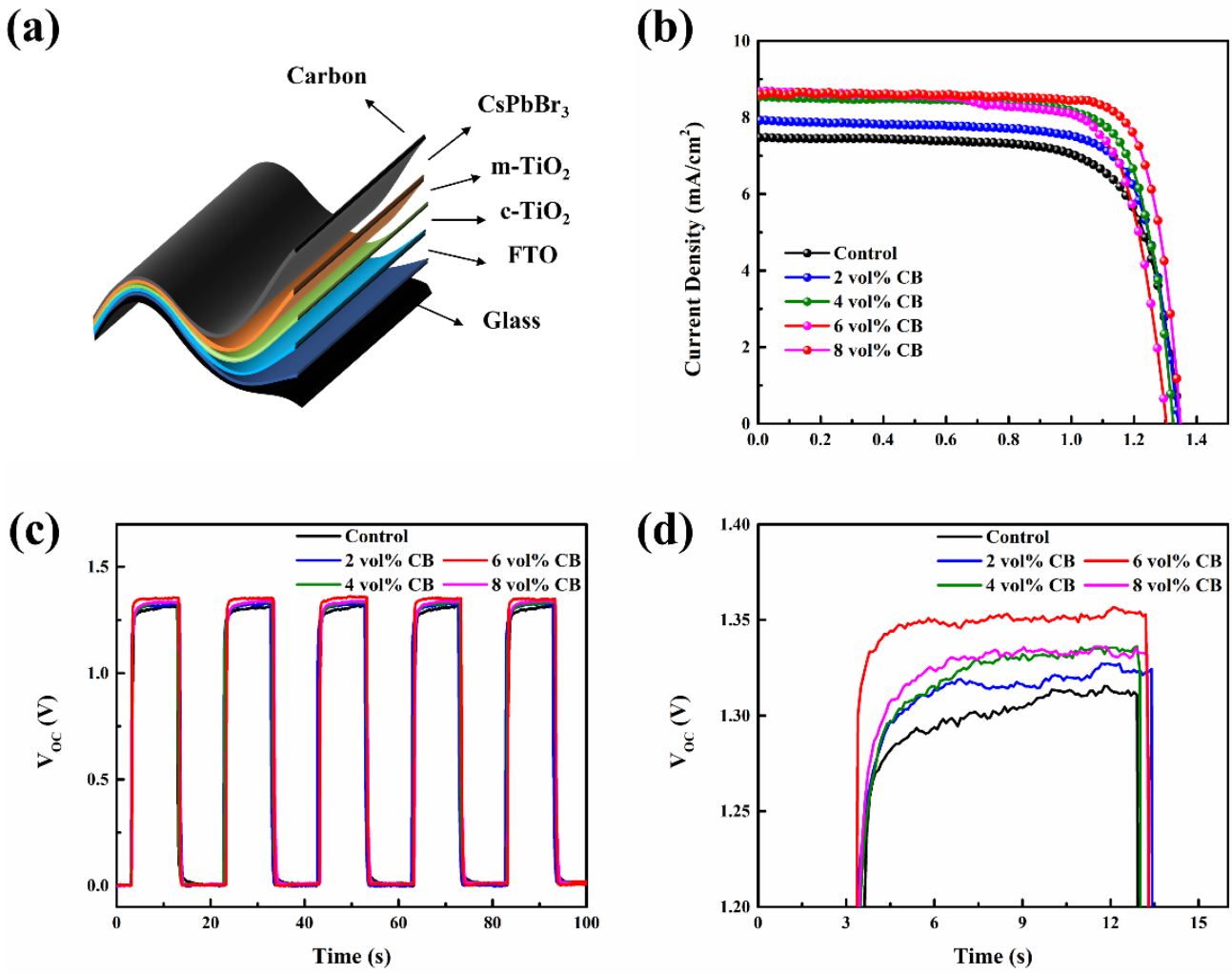

Fig. 7. $CsPbBr_3$ PSCs prepared without/with different amounts of CB: (a) device structure; (b) J-V; (c) optical response test diagram; (d) locally amplified optical response test diagram (colour online)

Table 1. Photovoltaic parameters of $CsPbBr_3$ PSCs prepared with different amounts of CB

Different amounts	V_{OC}/V	J_{SC} ($mAcm^{-2}$)	PCE/%	FF
Control	1.32	8.24	7.38	0.68
2 vol% CB	1.34	7.93	7.93	0.75
4 vol% CB	1.32	8.54	8.62	0.76
6 vol% CB	1.34	8.61	9.28	0.80
8 vol% CB	1.29	8.75	8.3	0.74

To further investigate the performance changes induced by CB treatment, space-charge-limited current (SCLC) measurements were conducted on $CsPbBr_3$ PSCs before and after CB treatment, as shown in Fig. 8(a). The SCLC data were analyzed using Origin software to obtain the trap-filled limit voltage (V_{TFL}), and the trap state density (N_{trap}) was calculated using Equation (1) [30, 31]:

$$N_{trap} = \frac{2\varepsilon_r \varepsilon_0 V_{TFL}}{qL^2} \quad (1)$$

where q is the elementary charge, ε_0 is the vacuum permittivity, ε_r is the relative permittivity, and L is the thickness of the perovskite film. Fitting analysis of the results revealed that the V_{TFL} values of the devices before and after CB treatment were 0.4642 V and 0.4113 V, respectively. Using Equation (1), the corresponding N_{trap} values were calculated to be $2.276\times10^{15}/cm^3$ and $1.370\times10^{15}/cm^3$, respectively, this significant reduction in trap state density after CB treatment suggests that CB improves the crystallinity of $CsPbBr_3$, thereby reducing near-band-edge defects.

To further elucidate the mechanism behind the improved device performance, dark J-V measurements were performed, as shown in Fig. 8(b). The dark current density at 0 V for the CB-treated device was approximately two orders of magnitude lower than that

of the untreated device, indicating that CB treatment effectively reduces reverse leakage current and non-radiative recombination.

Electrochemical impedance spectroscopy (EIS) was also conducted on the devices under a 0.8 V bias in the dark to study the carrier recombination process. The EIS spectra are shown in Fig. 8(c), with the corresponding equivalent circuit diagram provided in the inset. The diameter of the semicircular curve represents the recombination resistance (R_{rec}), where a smaller R_{rec} indicates more severe non-radiative recombination [32, 33]. The calculated R_{rec} of the CB-treated device exceeded 70 kΩ, while that of the untreated device was less than 30 kΩ. The fitting results clearly show that the R_{rec} of the CB-treated device was significantly larger, indicating that CB treatment effectively suppresses non-radiative recombination.

Maximum power point (MPP) steady-state output measurements were also conducted on devices before and after CB treatment, with results shown in Fig. 8(d). Analysis revealed that the steady-state output current density of the CB-treated device was approximately 7.89 mA/cm², higher than the 7.13 mA/cm² of the untreated device. Both devices maintained relatively stable output current densities over 200 s, demonstrating excellent stability. This further indicates that the $CsPbBr_3$ perovskite solar cells fabricated in this study possess outstanding stability.

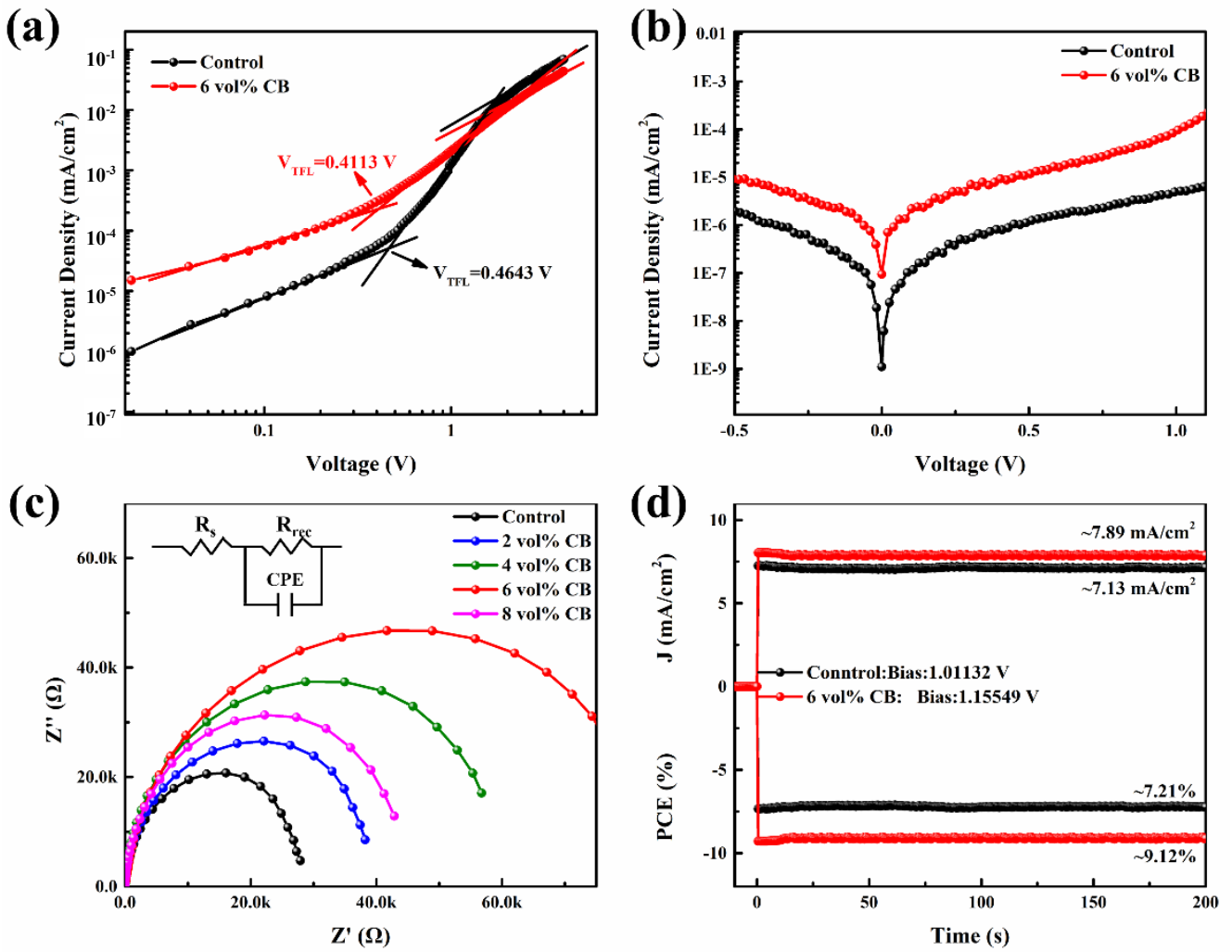

Fig. 8. Characteristics of $CsPbBr_3$ PSCs prepared with/without CB: (a) SCLC; (b) dark J-V; (c) EIS; (d) Steady-state photocurrent and PCE outputs at a voltage close to the maximum output point (colour online)

To further evaluate the long-term stability of devices with and without CB treatment, stability tests were conducted on unencapsulated devices stored in a dark air environment at approximately 20 °C and 20% relative humidity. The results are shown in Fig. 9. After 120 days of storage in air, the untreated devices retained 85% of their initial efficiency, while the CB-treated devices maintained over 90% of their initial efficiency. Based on the previous analysis, this improvement in stability is primarily attributed to the enhanced crystallinity of $CsPbBr_3$ films due to CB treatment, which effectively reduces the defect state density. Furthermore, the improved surface morphology and crystal quality of the $CsPbBr_3$ films contribute to the enhanced device stability.

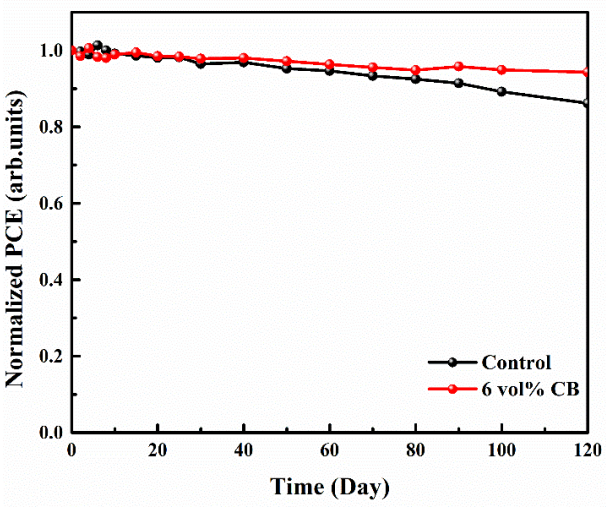

Fig. 9. Stability of $CsPbBr_3$ PSCs prepared with/without CB in air (colour online)

To ensure reproducibility and reliability of the experimental conclusions, 50 devices were fabricated under each condition. The photovoltaic parameters of the devices before and after CB treatment are presented in the box plots in Fig. 10. It is evident that the performance enhancement of CB-treated devices mainly originates from improvements in short-circuit current density (J_{SC}) and fill factor (FF). The CB additive passivated defects in the perovskite absorber layer and improved the crystallinity of $CsPbBr_3$ films, thereby enhancing J_{SC} and overall device performance.

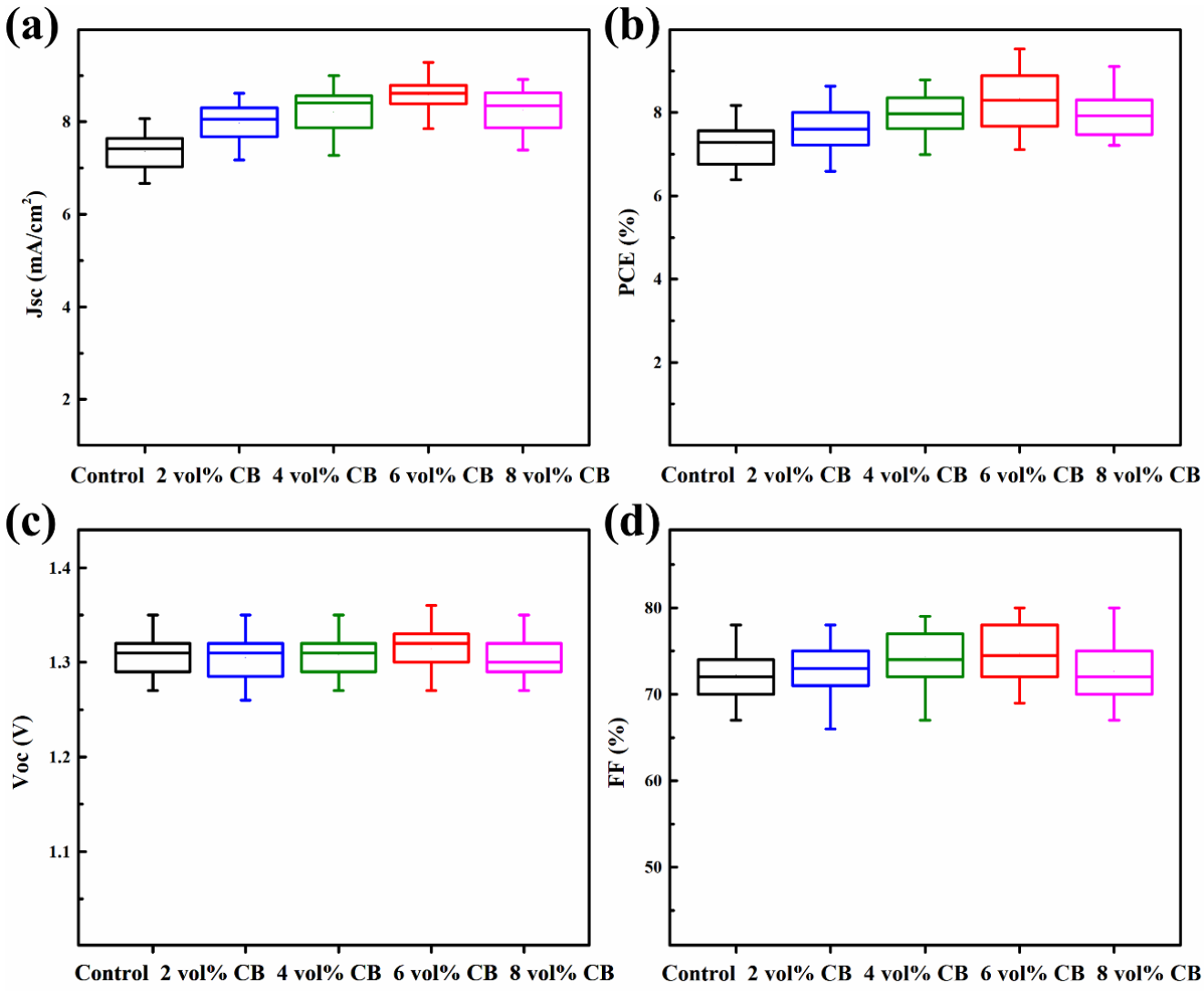

Fig. 10. Box attempts of (a) J_{SC}; (b) PCE; (c) V_{OC} and (d) FF for $CsPbBr_3$ PSCs prepared with different amounts of CB: 50 cell devices were prepared for each group (colour online)

4. Conclusion

In this study, the commonly used antisolvent CB was applied as an additive in $CsPbBr_3$ perovskite solar cells. Using a multi-step spin-coating process, CB was employed to regulate the growth of $CsPbBr_3$ films. The study found that CB optimizes the crystallization process of $PbBr_2$ films, thereby improving the morphology and crystallinity of $CsPbBr_3$ films. The CB-treated $CsPbBr_3$ films exhibited a more compact surface, larger grain size, lower trap state density, and higher crystallinity, which suppressed non-radiative recombination and improved the power conversion efficiency (PCE) and stability of the devices. At an optimal CB concentration of 6 vol%, the devices achieved a maximum efficiency of 9.28%. Furthermore, the unencapsulated devices retained over 90% of their initial efficiency after 120 days in an air environment.

Acknowledgments

This work was supported by the Fundamental Research Funds for the Central Universities (Grant No. 2652019121).

References

[1] S. Yang, W. Fu, Z. Zhang, H. Chen, C. Z. Li, J. Mater. Chem. A **5**(23), 11462 (2017).
[2] J. Duan, T. Hu, Y. Zhao, B. He, Q. Tang, Angew. Chem. Int. Ed. **57**(20), 5746 (2018).
[3] X. Zhao, T. Liu, A. B. Kaplan, C. Yao, Y. Loo, Nano Lett. **20**(12), 8880 (2020).
[4] S. Zhou, R. Tang, L. Yin, Adv. Mater. **29**(43), 1703682 (2017).
[5] M. Kulbak, S. Gupta, N. Kedem, I. Levine, T. Bendikov, G. Hodes, D. Cahen, J. Phys. Chem. Lett. **7**(1), 167 (2016).
[6] X. Liu, Z. Liu, X. Tan, H. Ye, B. Sun, S. Xi, T. Shi, Z. Tang, G. Liao, J. Power Sources **439**, 227092 (2019).
[7] J. Duan, Y. Zhao, B. He, Q. Tang, Angew. Chem. **130**(14), 3849 (2018).
[8] J. Duan, Y. Zhao, X. Yang, Y. Wang, B. He, Q. Tang, Adv. Energy Mater. **8**(31), 1802346 (2018).
[9] G. Su, B. He, Z. Gong, Y. Ding, J. Duan, Y. Zhao, H. Chen, Q. Tang, Electrochim. Acta **328**, 135102 (2019).
[10] G. Liao, J. Duan, Y. Zhao, Q. Tang, Solar Energy **171**, 279 (2018).
[11] S. Yang, W. Fu, Z. Zhang, H. Chen, C. Li, J. Mater. Chem. A **5**(23), 11462 (2017).
[12] B. Hu, J. Zhang, Y. Yang, Y. Dong, J. Wang, W. Wang, K. Lin, D. Xia, Chinese Chem. Lett. **35**(7), 108933 (2024).
[13] T. Liu, Y. Liu, X. Gao, J. Cao, Chinese Chem. Lett. **34**(8), 107883 (2023).
[14] K. Yan, Z. Shen, Y. Huang, B. Niu, H. Chen, C. Li, Chinese Chem. Lett. **35**(6), 109516(2024).
[15] T. S. Ripolles, P. Serafini, C. Redondo-Obispo, E. Climent-Pascual, S. Masi, I. Mora-Seró, C. Coya, Energy Technology **10**(3), 1 (2022).
[16] X. Liu, K. Yan, D. Tan, X. Liang, H. Zhang, W. Huang, ACS Energy Lett. **3**(11), 2701 (2018).
[17] J. Yang, Y. Chen, W. Tang, S. Wang, Q. Ma, Y. Wu, N. Yuan, J. Ding, W. Zhang, J. Energy. Chem. **48**(9), 217 (2020).
[18] N. Santhosh, R. I. Daniel, K. R. Acchutharaman, M. S. Pandian, P. Ramasamy, Mater. Today Commun. **31**, 103446 (2022).
[19] Y. Gou, S. Tang, C. Yun, P. Zhao, J. Chen, H. Yu, Mater. Horiz. **11**, 3465 (2024).
[20] I. M. Asuo, A. M. Varposhti, E. D. Gomez, N. Y. Doumon, Journal of Materials Chemistry C **12**(21), 7562 (2024).
[21] M. Kong, H. Hu, K. Egbo, B. Dong, L. Wan, S. Wang, Chinese Chem. Lett. **30**(6), 1325 (2019).
[22] R. Zhuang, L. Wang, J. Qiu, L. Xie, X. Miao, X. Zhang, Y. Hua, Chem. Eng. J. **463**, 142449 (2023).
[23] Z. Zhao, F. Gu, Y. Li, W. Sun, S. Ye, H. Rao, Z. Liu, Z. Bian, C. Huang, Adv. Sci. **4**(11), 1700204 (2017).
[24] C. Chen, H. Bala, S. Yao, B. Zhang, N. Sha, X. An, W. Zhang, D. Chen, J. Alloy. Compd. **920**, 165874 (2022).
[25] M. Yang, L. Zou, J. Cheng, J. Wang, Y. Jiang, H. Hao, J. Xing, H. Liu, Z. Fan, J. Dong, Acta Physica Sinica **72**, 168101 (2023).
[26] C. F. J. Lau, X. Deng, J. Zheng, J. Kim, Z. Zhang, M. Zhang, J. Bing, B. Wilkinson, L. Hu, R. Patterson, S. Huang, A. Ho-Baillie, J. Mater. Chem. A **6**(14), 5580 (2018).
[27] Y. Pei, H. Guo, Z. Hu, J. Zhang, Y. Zhu, J. Alloy. Compd. **835**, 155283 (2020).
[28] J. Peng, Y. Wu, W. Ye, D. A. Jacobs, H. Shen, X. Fu, Y. Wan, N. Wu, C. Barugkin, H. T. Nguyen, D. Zhong, J. Li, T. Lu, Y. Liu, M. Lockrey, K. Weber, K. Catchpole, T. White, Energ. Environ. Sci. **10**(8), 1792 (2017).
[29] S. Chen, J. Dong, J. Wu, S. Hou, J. Xing, H. Liu, H. Hao, Sol. Energ. Mat. Sol. C **201**, 110110 (2019).
[30] J. Ma, Y. Li, J. Li, J. Qin, M. Wu, X. Lv, Z. Hsu, Y. Lu, X. Wu, Y. Fang, J. Guo, Nano Energy **75**, 104933 (2020).
[31] Z. Liu, T. Shi, Z. Tang, S. Bo, G. Liao, Nanoscale **8**(13), 7017 (2016).
[32] X. Wang, F. Sun, G. Yin, Y. Wang, L. Bo, M. Dong, Sensors **18**(2), 330 (2018).
[33] Q. Jiang, Y. Zhao, X. Zhang, X. Yang, Y. Chen, Z. Chu, Q. Ye, X. Li, Z. Yin, J. You, Nat. Photonics **13**(7), 460 (2019).

*Corresponding author: jjdong@cugb.edu.cn